Materials Characterization 127 (2017) 129–136

Contents lists available at ScienceDirect

Materials Characterization

journal homepage: www.elsevier.com/locate/matchar

The relation between aging temperature, microstructure evolution and hardening of Custom 465® stainless steel

Sigalit Ifergane [a,b], Malki Pinkas [b], Zahava Barkay [c], Eli Brosh [b], Vladimir Ezersky [d], Ofer Beeri [b], Noam Eliaz [a,*]

[a] Department of Materials Science and Engineering, Tel-Aviv University, Ramat Aviv, Tel Aviv 6997801, Israel
[b] Nuclear Research Center Negev, P.O. Box 9001, Beer Sheva 84100, Israel
[c] The Wolfson Applied Materials Research Centre, Tel-Aviv University, Ramat Aviv, Tel Aviv 6997801, Israel
[d] Ilse Katz Institute for Nanoscale Science and Technology, Ben-Gurion University, Beer-Sheva 84105, Israel

ARTICLE INFO

Article history:
Received 2 July 2016
Received in revised form 11 January 2017
Accepted 24 February 2017
Available online 27 February 2017

Keywords:
Dilatometry
Precipitation hardened martensitic stainless steel
Transmission Kikuchi diffraction (TKD)
Transmission electron microscopy (TEM)
Phase transitions
Aging

ABSTRACT

The microstructure and hardness of Custom 465® precipitation hardened stainless steel were characterized following 4 hours aging at temperatures ranging from 482 °C to 648 °C. Dilatometry measurements and thermodynamic calculations were used to understand the mechanism of martensite-to-austenite reversion. Three major stages of aging were observed. The first stage is the peak hardening at aging temperatures of 480–510 °C, where both η-Ni_3Ti precipitation and austenite reversion begin independently of each other. The second stage is the initial stage of overaging observed above 538 °C as reduction in hardness is due to a slight increase in both the precipitate dimensions and the reverted austenite volume fraction. The third, progressive overaging stage occurs above 593 °C in which a dramatic hardness decrease is caused by a significant increase in both precipitate dimensions and reverted austenite volume fraction. Transmission Kikuchi diffraction orientation mapping revealed that globular austenite randomly nucleates at martensite grain boundaries, while acicular austenite nucleates along martensite lath boundaries. Thermodynamic calculations indicated that the dissolution of η-Ni_3Ti precipitates does not govern the austenite reversion, although both phases are in competition for Ni. While the thermodynamic calculation predicts increase in the fraction of austenite with increase in aging temperature, the fraction of austenite found at room temperature in aged samples does not vary when the aging temperature, in which austenite reversion occurs, is increased above 593 °C. This is explained by the change in composition of the austenite as a function of aging temperature.

1. Introduction

Custom 465® precipitation hardened (PH) stainless steel is a martensitic age-hardened alloy characterized by a combination of high strength, high fracture toughness and good resistance to general corrosion and stress corrosion cracking (SCC), compared with other high-strength PH stainless steels such as Custom 455 and Carpenter 13–8 [1]. Hardening of Custom 465® upon aging is attributed to the formation of the intermetallic hexagonal η-Ni_3Ti phase in the form of rod-shaped nano-precipitates [2]. The formation of rod-shaped η-Ni_3Ti precipitates is typical to Ti-containing Ni-rich maraging steels, such as C250 and T250 [3–8], Fe-20Ni-1.8Mn-1.6Ti-0.59Al [9], Fe-10Cr-10Ni-2 W [10] and Fe-25.3Ni-1.7 Ti [11] alloys (all concentrations are presented in wt%).

Retained austenite is the untransformed austenite that remains stable after quenching from the austenitizing temperature to room (or subzero) temperature; it is the result of a martensite finish temperature below room temperature, and it generally forms randomly between martensite laths in PH steels. In contrast, *reverted austenite* forms during a subsequent tempering or aging treatment, usually in localized areas. Its occurrence depends on chemical composition, the applied aging temperature and time. In a previous study we reported the formation of reverted austenite during aging of Custom 465® at 480 °C for 4 h [2]. The formation of reverted austenite has been reported for various maraging steels; its morphology is characterized by coarse, patchy regions at martensite lath boundaries [4,8,12]. The orientation relationship between martensite and austenite corresponds to the Kurdjumov-Sachs relationship: a parallelism between the close-packed planes and directions in the two structures. The formation of reverted austenite is the result of a change in the equilibrium concentration of austenite in the alloy. Yet, it is not clear whether this change is solely a function of the temperature, or it is due to local Ni enrichment at temperatures exceeding the stability range of these precipitates. For example, for maraging C250 steel it was demonstrated that the formation of reverted austenite is due to the dissolution of Ni_3Mo precipitates, which locally enrich the matrix with Ni [3].

* Corresponding author.
E-mail address: neliaz@tau.ac.il (N. Eliaz).

http://dx.doi.org/10.1016/j.matchar.2017.02.023
1044-5803/

According to previous studies [13,14], increasing the aging temperature of Custom 465® results in lower hardness and strength values, while fracture toughness and corrosion resistance are improved. A detailed study of the microstructure evolution upon aging of Custom 465® at different temperatures is essential for the understanding of the relation between aging temperature and the resulting mechanical properties and corrosion behavior. A comprehensive characterization of the microstructure in general, and of potential traps for diffusing hydrogen specifically, is important also for our on-going study of hydrogen permeation through this steel. However, to the best of our knowledge, such thorough characterization is not reported in the literature. Also, the austenite fraction as a function of aging temperature has not been correlated with the evolution of the η-Ni_3Ti phase. To reach these goals, the microstructure of Custom 465® was characterized following aging at temperatures ranging from 482 °C to 648 °C, focusing on the η-Ni_3Ti precipitate dimensions and the fraction of austenite and its location. Dilatometry measurements and thermodynamic calculations were employed to gain a better understanding of the phase transformations occurring during aging treatments.

2. Experimental procedures

2.1. Thermomechanical treatments and microstructure characterization

Custom 465® stainless steel in the form of a 2-inch diameter rod was purchased from Carpenter Technology (Wyomissing, PA). The composition of this steel was determined by Inductively Coupled Plasma Atomic Emission Spectroscopy (ICP-AES) analysis as (wt%): Fe–10.7Cr–10.9Ni–0.86Mo–1.4Ti–0.04Al–0.04Zn–0.0046C. The rod was received in the solution annealed (SA) at 900 °C followed by cold-treatment at −73 °C for 8 h within 8 h from the SA treatment. All specimens were cut transversally to the rod axis.

0.5–1.0 mm thick specimens were aged at several temperatures, corresponding to the definition of aging treatments of Custom 465®: 482 ± 5 °C (H900), 510 ± 5 °C (H950), 538 ± 5 °C (H1000), 560 ± 5 °C (H1040), 593 ± 5 °C (H1100), 648 ± 5 °C (H1200). In addition, hardness test was conducted on the 460 ± 5 °C (H860) sample in order to determine the peak hardness. All aging treatments were conducted in an argon shielding atmosphere. Four hours aging durations were chosen, for comparison with other works dealing with the same alloy [13,14]. The heating and cooling rates were 10 °C/min and 40–60 °C/min, respectively, in a tube furnace. During cooling, the samples were drawn away from the heated zone and kept within the furnace atmosphere. Thermocouple was attached to the specimen during all stages of heating and cooling. After aging, the specimens were ground and polished on both sides down to 1 μm. For each treatment, microhardness test was done on 2–3 specimens, with 5 repetitions on each specimen, using Vickers microhardness machine (Shimadzu GmbH HMV-2 T) and 200 g load. The volume fraction of reverted austenite was measured by X-ray diffraction (XRD). A PANalytical Empyrean Powder diffractometer equipped with a position sensitive (PSD) PIXCEL detector and Cu-Kα radiation was used. A graphite secondary monochromator was used to reduce fluorescence effects and improve the signal-to-noise and signal-to-background ratios. The relative quantities of reverted austenite were determined from X-ray diffraction patterns according to standard method ASTM E975 [15] for X-ray determination of retained austenite in steel with near-random crystallographic orientation, using the integrated intensities of X-ray diffraction peaks.

Samples for transmission electron microscopy (TEM) and transmission Kikuchi diffraction (TKD) in a scanning electron microscope (SEM) were mechanically polished to a 30-μm thickness on a 1000 grit SiC grinding paper, and polished with 6 μm and 1 μm diamond pastes. Disks, 3 mm in diameter, were cut by a punch, and the central area of the disk sample was ion-milled to electron transparency using a Gatan Precision Ion Polishing System (PIPS).

JEOL JEM-2100F TEM equipped with an energy-dispersive X-ray spectrometer (EDS) system model JED 2300T was used. Analysis of reverted austenite was done by TKD in a Quanta 200 FEG environmental SEM (ESEM) for orientation mapping, using an Oxford Aztec System with Nordlys II detector.

2.2. Phase transformations – dilatometry

The initial density of the alloy was measured by Archimedes method as 7.777 ± 0.003 g/cm^3. Dilatometry measurements were conducted in order to identify the sequence of phase transformations that take place during aging. Relatively slow heating and cooling rates were assigned in order to achieve conditions which favor thermodynamic stability. The heating rate was 4 °C/min, and the holding time was 30 min at 900 °C, followed by cooling to room temperature at 10 °C/min. The chosen rate of 4 °C/min is a compromise between the low heating rates needed for measurement accuracy (see ASTM E228) and the faster heating rates used for arriving at aging temperature during the thermal treatments. Dilatometry was done using a Linseis-L75 system. The specimen holder and the piston were made of fused silica. The range of extension measurement was ±250 μm. The length, time and temperature information were recorded at microsecond intervals, and the vacuum was attained at 10^{-2} mbar using a rotation pump. Afterward, 1 bar helium atmosphere was filled to facilitate thermal conduction in the instrument. For calibration, the same procedure was followed with pure Fe (99.999%), albeit with a higher initial vacuum of 10^{-5} mbar, using a diffusion pump. Specimens were of 4 × 4 × 20 mm dimensions. The surface was ground on both sides by SiC papers down to 600 grit, followed by polishing down to 1 μm using diamond paste. The parallelism of the measured surfaces was ±0.05 μm.

3. Results

3.1. Microstructure characterization

The changes in hardness, precipitate dimensions and relative volume of reverted austenite upon aging are shown in Tables 1 and 2 and in Fig. 1. Hardness measurements (Table 1) show an increase upon aging relative to the SA condition, from 327 ± 5 VHN in the SA condition to 616 ± 18 VHN in the aged (480–510 °C) condition. As the aging temperature is raised, a lower extent of hardness increase is obtained. In the range 480–550 °C, a decrease in hardness of Custom 465® as the aging temperature is increased has been reported before [13,14].

Selected area electron diffraction (SAED) patterns acquired in the TEM revealed two phases: martensite with a body-centered cubic (BCC) structure and hexagonal η-Ni_3Ti. A representative SAED pattern is shown in Fig. 2. Bright-field (BF) images of aged specimens and their corresponding dark-field (DF) images are shown in Fig. 3. The orientation relationship between the Ni_3Ti precipitates and the martensite matrix was calculated from Fig. 2 as $\{011\}_M//\{0001\}_{Ni3Ti}$ and $\{111\}_M//11\bar{2}0_{Ni3Ti}$. In the BF-TEM images in Fig. 3 one can observe the three variants of η-Ni_3Ti precipitates, at an angle of 60° relative to

Table 1
Vickers hardness measured at 200 g, and after conversion to HRC values. Values are compared to reported measured data.

Aging temp. (°C)	Condition	HVN	HRC[a]	Ref. 13 (HRC)	Ref. 14 (HRC)
460	H860	567 ± 10			
480	H900	615 ± 11	56	54	–
510	H950	616 ± 18	56	54	49.5
538	H1000	548 ± 13	52	52	47.5
560	H1040	547 ± 7	52	51	45.5
593	H1100	481 ± 6	48	–	–
648	H1200	381 ± 6	39	–	–

[a] Converted according to ASTM E140–12.

Table 2
Reverted austenite quantified by XRD, and η-Ni_3Ti precipitate dimensions for the different aging treatments, as presented in Figs. 1, 3–5. The Ni_3Ti precipitate dimensions are based on averaging of minimum 5 precipitates. Thermodynamic computation of the fractions of η-Ni_3Ti precipitates and austenite.

Aging temp. (°C)	Reverted austenite	Diameter of Ni_3Ti	Length of Ni_3Ti	Calculated equilibrium fraction (at%)	
	(vol%)	D (nm)	L (nm)	Ni_3Ti	Austenite
480	3.4 ± 0.2	2.8 ± 0.4	7 ± 1	6.5	3.1
510	4.7 ± 0.1	4.4 ± 0.7	14 ± 2	6.5	4.2
538	5.2 ± 0.4	7.6 ± 1	32 ± 7	6.4	6.7
560	6.0 ± 0.7	9.8 ± 2	39 ± 8	6.2	11.4
593	15.5 ± 0.9	13 ± 2	68 ± 13	5.85	19.0
648	19.3 ± 1.7	26 ± 4	128 ± 37	3.4	58.9

each other, as reported for Fe-20Ni-5Mn alloy [16]. A DF image taken at the $(22\bar{4}0)$ η-Ni_3Ti plane, which is parallel to the long axis of one of the variants of precipitates, revealed a rod-shaped morphology. For each aging treatment the diameters and lengths of precipitates were measured from DF images obtained at identical crystallographic orientation: the $(22\bar{4}0)$ η-Ni_3Ti reflection at $[112]_M$ zone axis of martensite. The results (Table 2 and Fig. 1a & b) indicate that the dimensions of η-Ni_3Ti increase with the temperature of aging.

The fraction of reverted austenite that remains after cooling to room temperature was characterized by mapping its location in the steel using nano-scale imaging by TKD in SEM (Fig. 4) and quantified based on XRD patterns (Fig. 1c, Fig. 5). For all aging treatments, reverted austenite is noticed at both grain boundaries and inter-lamella interfaces. In addition, tiny parts could be observed at boundaries inside lamellae, which could also be inter-lamellae interfaces above or below the plane of the image. Sinha [17] reported preferred transformation of austenite along dislocation pile-ups inside lamella. Song et al. [18] reported that in PH 13–8Mo steel the austenite morphology is globular at grain boundaries and acicular at lath boundaries, similar to our results.

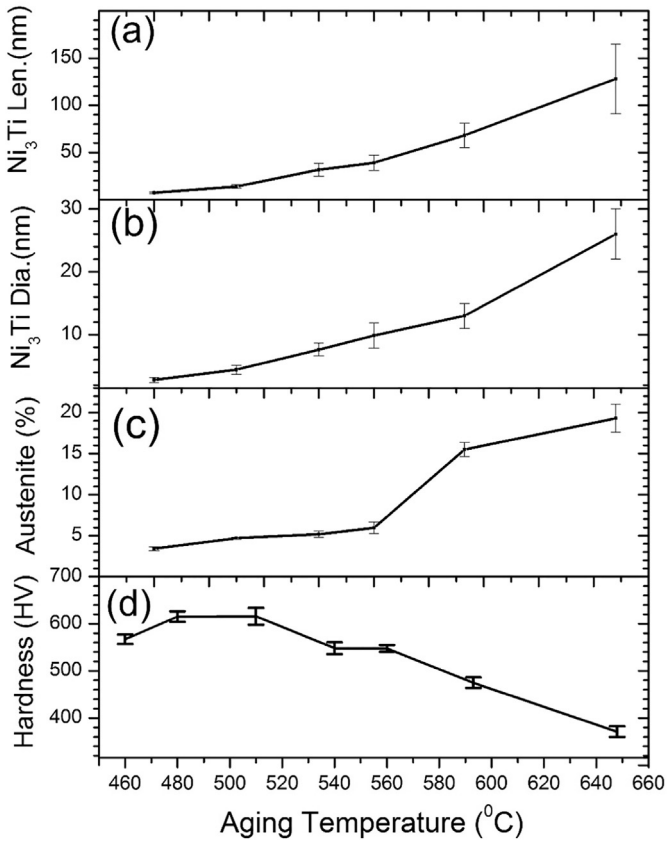

Fig. 1. The effect of aging temperature on precipitate dimensions – length (a) and diameter (b) – as measured from the $(22\bar{4}0)$ reflection of η-Ni_3Ti precipitates in TEM electron diffraction patterns. (c) Reverted austenite volume fraction, as measured by XRD at room temperature. (d) Vickers hardness.

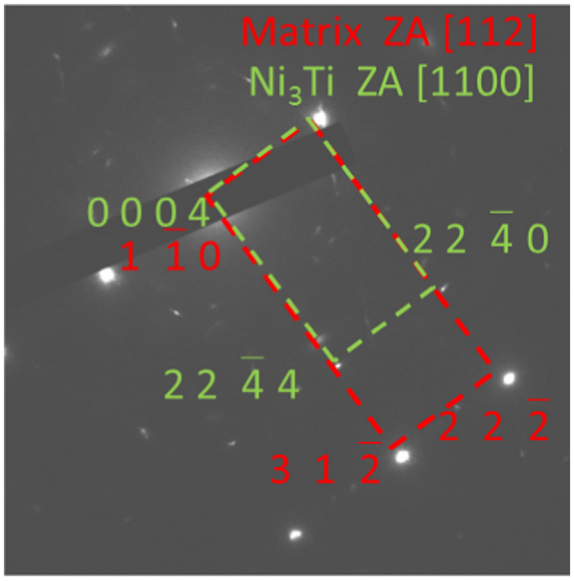

Fig. 2. TEM electron diffraction pattern at zone axis $[112]_M$. Orientation relation between η-Ni_3Ti and martensite is demonstrated in a sample aged at 560 °C.

XRD patterns of the alloy in its solution annealed condition and following 482 ± 5 °C (H900) and 593 ± 5 °C (H1100) aging treatments are shown in Fig. 5. The austenite volume fraction, as determined from XRD patterns, is increasing with aging temperature (Fig. 1c, Table 2). The ASTM E975 standard method was applicable for determining the austenite volume fraction since in all diffractograms the two phases, austenite and martensite, display random orientation as can be concluded from the reflection intensities, which correspond to Pearson's crystal data (#1927926 for austenite, #455184 for martensite). It should also be noted that the background counting is ~100–200 counts, which is about 4 orders of magnitude lower than the strongest martensite reflection (110) in each diffractogram.

Some increase in the fraction of reverted austenite, from 3.2 ± 0.2 vol% to 5.9 ± 0.2 vol%, which is of the same order of magnitude as the accuracy of measurement, was observed as the aging temperature was raised from 482 °C to 560 °C, respectively. At higher aging temperatures, the austenite fraction increased abruptly, reaching a value of 15 vol% in the sample aged at 593 °C. A similar value of ~19 ± 1.7 vol% was measured in the sample aged at 648 °C.

3.2. Dilatometry measurements

A typical dilatometry curve obtained at a heating rate of 4 °C/min is shown in Fig. 6. Constructed tangents to the curve were used to identify the start and finish points of the transformations and to quantify the extent of contraction occurring due to transformations. Two transformations can be identified in the dilatometry curve, as will be explained below. Following the interpretation of dilatometry curves of other PH-steels [4,19,20,21], the first transformation was attributed to the precipitation of η-Ni_3Ti, whereas the second to the reversion of martensite to austenite. As heating proceeds, the sample demonstrates a linear expansion up to ~470 °C, where a small contraction is observed, indicating the start of precipitation at this temperature (P_s). Precipitation finishes (P_f) when the linear expansion is resumed, at a temperature of about 605 °C. The deviation from linearity at 640 °C indicates the start of austenite

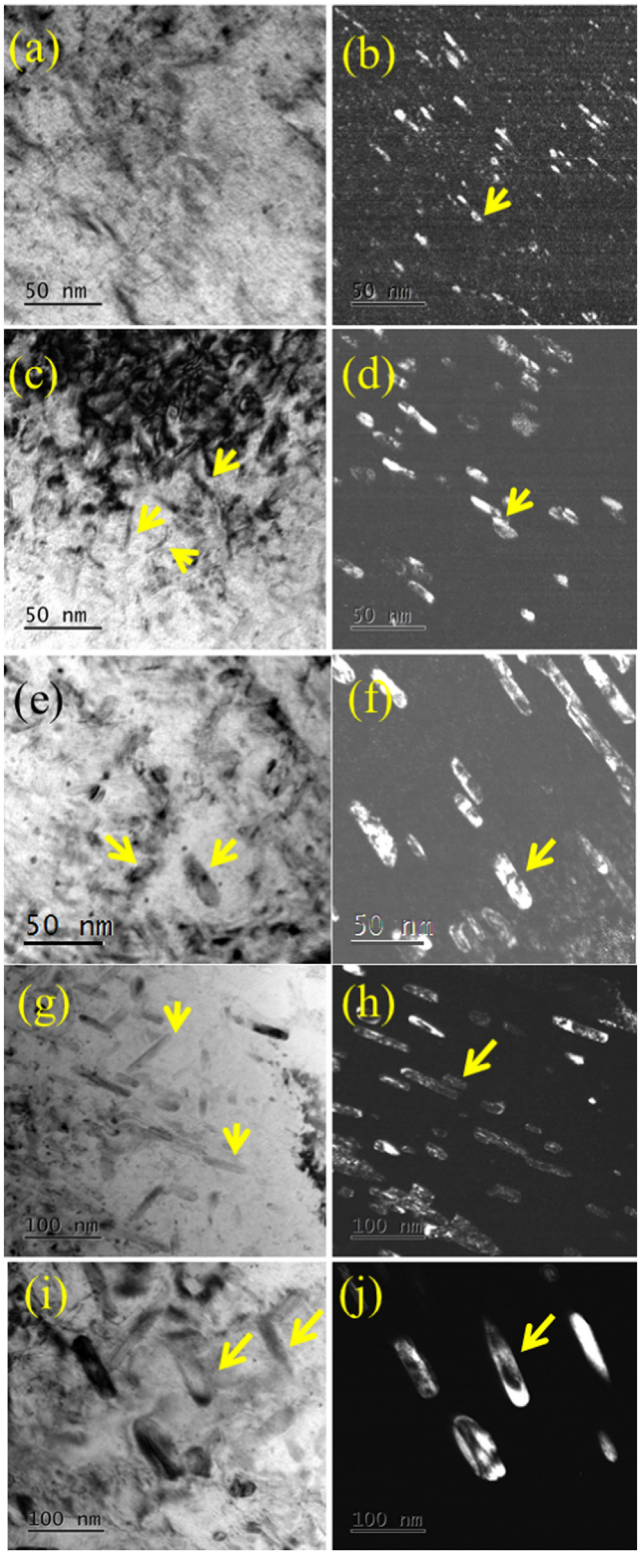

Fig. 3. TEM images (a, c, e, g, i - BF; b, d, f, h, j - DF) taken at zone axis $[112]_M$. Three variants of precipitates are marked by arrows. DF images are from the $(22\bar{4}0)$ reflection of one variant of the η-Ni_3Ti precipitates. Aging at 482 °C (a, b), 538 °C (c, d), 560 °C (e, f), 593 °C (g, h), and 648 °C (i, j).

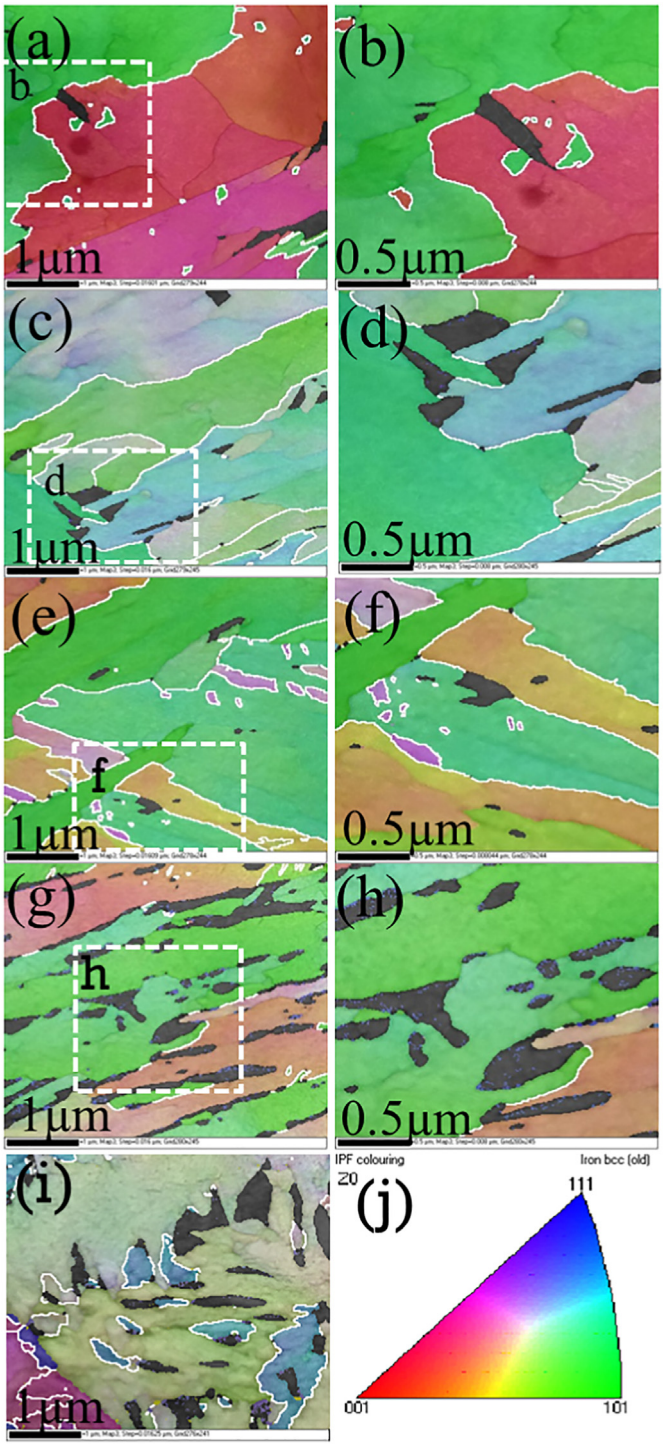

Fig. 4. Surface normal-projected inverse pole figure (IPF) orientation maps (a–i) and IPF colored map (j) using TKD method in SEM for aged specimens: 480 °C (a, b), 510 °C (c, d), 560 °C (e, f), 593 °C (g, h), and 648 °C (i). Interlamella interface at misorientation 60° is marked in white, whereas reverted austenite is colored in black. Step sizes are 16 nm for (a, c, e, g, i) and 8 nm for (b, d, f, h).

reversion (A_s), which finishes (A_f) at 740 °C. A complete solution is ensured by heating continuously up to 900 °C and holding at this temperature for 1 h. During cooling, the sample is contracted linearly with temperature, down to 28 °C, at which drastic expansion is observed, thus identified as the martensite starting temperature (*Ms*). This value is comparable with the one calculated according to the composition of the steel from the empirical equation suggested in [22] and given in Eq. (1), which yields a value of 39 °C:

$$Ms(°C) = 539 - 423[C] - 30.4[Mn] - 17.7[Ni] - 12.1[Cr] - 7.5[Mo]\ [wt\%] \quad (1)$$

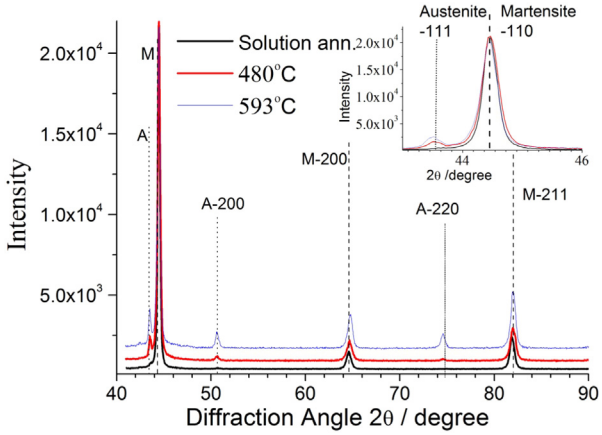

Fig. 5. XRD patterns normalized according to the highest martensite M (110) peak in each pattern. Martensite BCC phase is evident in all three sample types: SA (black), 480 °C (red), and 593 °C (blue). Austenite FCC phase is distinguished in heat-treated samples, as can also be seen in the inset focusing on the (111) austenite and (110) martensite reflections. (For interpretation of the references to color in this figure legend, the reader is referred to the web version of this article.)

The slope of the cooling curve does not regain linearity during cooling to room temperature, indicating that the martensitic transformation was not complete. The martensite finishing temperature (M_f) is expected to be lower than room temperature, which is the reason for the cold-treatment at −76 °C performed by the manufacturer of the steel.

The contraction P_C due to η-Ni_3Ti precipitation, and A_C due to the martensite-to-austenite transformation, as marked in Fig. 6b, are 0.035% and 0.14%, respectively. Similar values (0.02% and 0.14%, respectively) were reported for 17–4 PH stainless steel [21], implying that the extents of precipitation and of reverted austenite are similar.

3.3. Thermodynamic calculations

Knowing the equilibrium state to which the system is striving at each aging temperature is important for the understanding of the phase transformations that occur during the aging cycle. For this purpose, thermodynamic calculations were carried out using Thermo-Calc software [23] with the TCFE7 Steels/Fe-alloys database [24]. Here we shall refer to *metastable equilibrium*, i.e., a state that may be changing, although too slowly to be observed. Such a system would undergo a large change in its properties when subjected to some small disturbance. It is neither paraequilibrium (because the concentration of fast-diffusing carbon and nitrogen is negligible in the Custom 465® steel) nor orthoequilibrium (because some phases are assumed not to form). Equilibrium calculations done for the composition of Custom 465® steel at $T = 648$ °C (H1100) revealed that the equilibrium phases are FCC_A1 (austenite) and Laves_C14 phase consisting primarily of Fe, Ti and Ni. At lower temperatures, equilibrium calculations lead to prediction of η-Ni_3Ti precipitates, which were indeed observed in the present study, but also a miscibility gap in the BCC_A2 (ferrite) between Cr-rich and Fe-rich compositions and appearance of *P*-phase [25] composed of Mo, Ni and Cr. These predictions represent equilibrium states, as demonstrated in a recent study on maraging steels, where the predicted equilibrium phases were found in a specimen held at 510 °C for 1200 h [3]. The short-term thermal treatments in the present study are evidently not sufficient to reach full equilibrium state. Hence, in order to obtain a better representation of the real situation, calculations were performed with the following constraints: only BCC_A2 (corresponding to martensite), FCC_A1 (corresponding to austenite) and η-Ni_3Ti phases may be stable, and no split of the BCC_A2 phase into two different compositions is allowed. The above constraints define

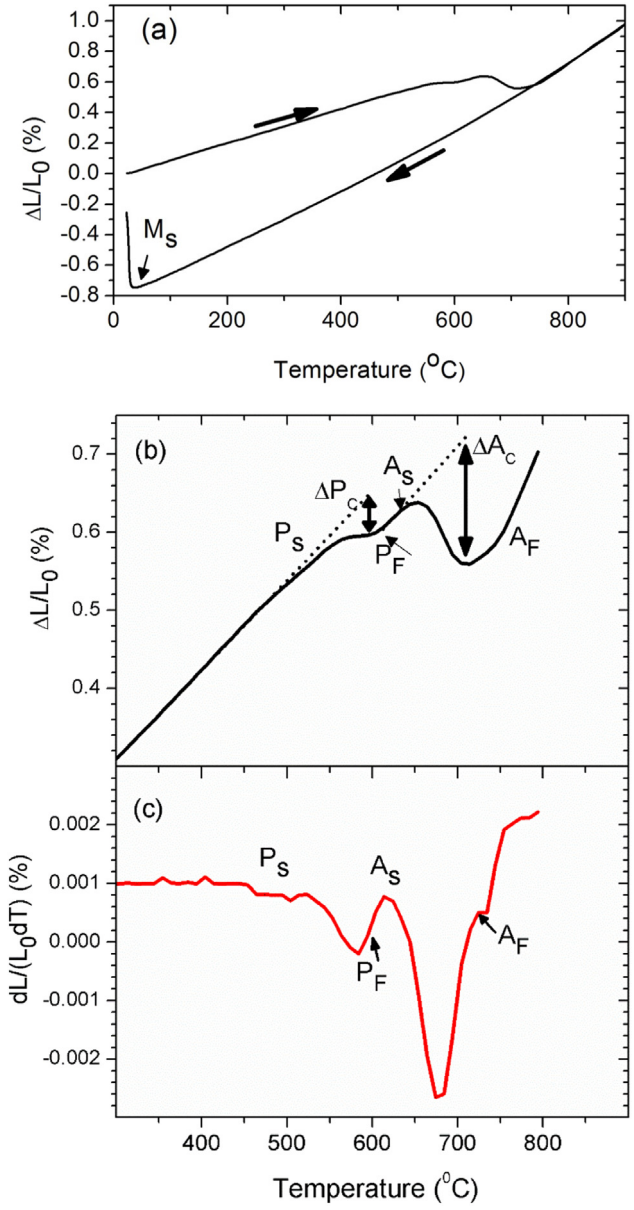

Fig. 6. Dilatometry curve measured at heating rate of 4 °C/min and cooling rate of 10 °C/min. (a) $\Delta L/L_0$ vs. temperature for heating and cooling. (b) $\Delta L/L_0$ vs. temperature for heating only, within a narrower temperature range. (c) Relative length change $dL/(dt \cdot L_0)$ vs. temperature during heating. The constructed tangents to the curve are used to identify the start/finish of the Ni_3Ti precipitation P_S/P_f, and austenite transformations A_s/A_f, respectively. In addition, ΔP_C and ΔA_C, which are used to calculate the contraction due to η-Ni_3Ti precipitation and martensite-to-austenite transformation, respectively, are marked.

calculations of metastable equilibria[1]. The calculated phase content is shown in Fig. 7 and Table 2. According to these calculations, the η-Ni_3Ti phase should exist up to 700 °C, but should disappear at higher temperatures. Indeed, this phase was identified in all samples treated at temperatures as high as 648 °C, but was negligible in the steel in its as-received condition [2], which according to the manufacturer datasheet was quenched from 900 °C. The calculations show that the formation of austenite does not stem from the dissolution of Ni_3Ti, since the increase in austenite occurs prior to the dissolution of Ni_3Ti.

[1] Such metastable equilibria are not complete equilibrium (the latter also called orthoequilibrium), but are also not to be confused with other types of metastable equilibria, such as paraequilibrium.

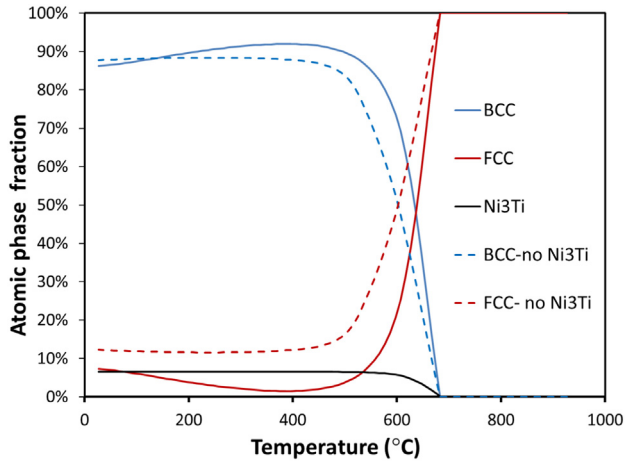

Fig. 7. Calculated phase fractions of martensite (BCC) and austenite (FCC) as a function of temperature in the presence of η-Ni_3Ti (continuous lines), and in the hypothetic case of absence of η-Ni_3Ti (dashed lines).

The austenite (FCC) phase is predicted to persist all over the range of aging temperatures, although its fraction is predicted to change, decreasing from its room-temperature value down to a minimum at around 400 °C, and increasing rapidly above ~580 °C, reaching an asymptote at 680 °C. These values are in line with the measured A_s temperature of 640 °C. The predicted amount of reverted austenite is listed in Table 2. Note that the thermodynamic calculations refer to the amount of austenite at the aging temperature in which reversion occurs, while the amount measured from XRD patterns relates to the reverted austenite at room temperature. Since there is a negligible amount of FCC phase in the solution annealed and subsequently rapidly cooled to subzero temperature specimens [2], most of the FCC phase detected in the aged specimens must have formed during the thermal treatments undertaken in the present work.

The dilatometry measurements show that the precipitation of η-Ni_3Ti is prior to the reversion of austenite. This raises a question about the effect of the formation of η-Ni_3Ti on the martensite-to-austenite phase transformation. To answer this question, the phase calculations were repeated, adding a constraint that the formation of η-Ni_3Ti should be suspended so that only FCC_A1 and BCC_A2 phases are included in the metastable equilibrium calculation. The austenite fraction as a function of temperature (Fig. 7) follows the same trend for both calculations, but the fraction of austenite is higher when the η-Ni_3Ti is suspended. In Fig. 8 the composition of the austenite (FCC_A1) phase is shown for both

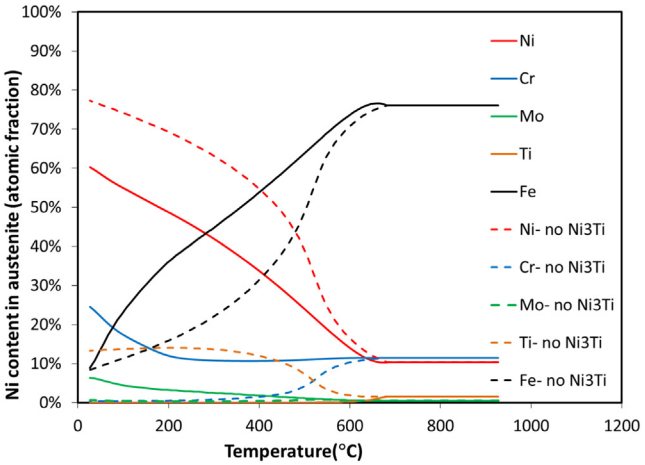

Fig. 8. Calculated composition of austenite (FCC) as a function of temperature in the presence of η-Ni_3Ti (continuous lines), and in the hypothetic case of absence of η-Ni_3Ti (dashed lines).

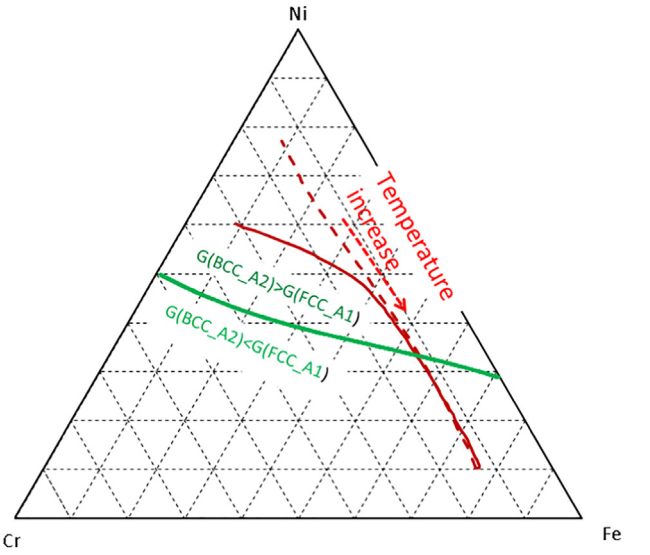

Fig. 9. Calculated trajectory of the composition of austenite plotted on Cr-Fe-Ni composition triangle (minor alloying elements are counted with Cr), with η-Ni_3Ti included (continuous red line), or with η-Ni_3Ti suspended (dashed red line). The locus of zero driving force for martensitic transformation is represented by a green line. (For interpretation of the references to color in this figure legend, the reader is referred to the web version of this article.)

calculations, i.e. either with η-Ni_3Ti or in the hypothetic case without η-Ni_3Ti. One can notice that in the hypothetic calculation, the Ni content in austenite is higher for all temperatures. Thus, we can conclude that while the formation of austenite does not stem from the precipitation or dissolution of Ni_3Ti, and *vice versa*, the two phases compete for Ni in their formation even though there is enough Ni to form both. It is also seen that, in both calculations, austenite formed at lower temperature is richer in Ni.

In Fig. 9, the trajectory of the change of the composition of austenite is plotted on a Cr-Fe-Ni composition triangle (the other alloying elements are grouped with Cr for simplicity, although the real composition was used for computations). As aging temperature increases, the composition of austenite moves from a region where at room temperature the Gibbs energy of the BCC phase, G(BCC), is higher than that of the FCC phase, G(FCC), to a region where at room temperature G(BCC) is lower than G(FCC). The locus where G(FCC) = G(BCC) at room temperature is shown in Fig. 9 as a green line[2]. As illustrated in Fig. 10a, the driving force for martensite transformation at room temperature, G(FCC)-G(BCC)[3], is increasing with the austenite aging temperature. This means that austenite that is formed at higher temperatures will undergo martensitic transformation to BCC more readily upon rapid cooling to room temperature, while austenite that is formed at lower temperatures is expected to remain at room temperature.

The change in stability of the reverted austenite with respect to martensitic transformation can be deduced not only from the theoretical thermodynamic calculation of driving force, but also from the calculation of the *Ms*-temperature from the empirical formula, Eq. (1). From the formula one can see that *Ms* decreases with the content of the alloying elements (Cr, Ni, and Mo) in austenite. Therefore, Fig. 10b presents the *Ms* calculation according to the predicted austenite composition (Fig. 8) as a function of aging temperature. Reverted austenite

[2] In other terms, this is the locus of compositions where T_0 for the BCC-FCC transformation is room temperature.

[3] A transformation is thermodynamically favored if it reduces the Gibbs energy. When the driving force is determined as G(FCC)-G(BCC), we refer to both phases as having the same chemical composition. A positive value indicates a thermodynamically favored reaction, and *vice versa*.

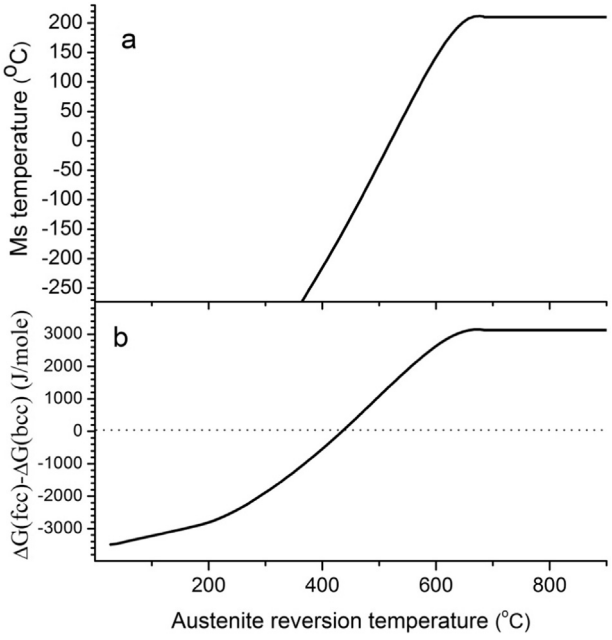

Fig. 10. Stability of austenite-martensitic transformation. (a) Driving force for martensitic transformation versus austenite reversion temperature (aging temperature). (b) *Ms* temperature as a function of reversion temperature.

that is formed at high temperature, and therefore contains less alloying, has higher *Ms* so it is likely to transform to martensite upon cooling.

4. Discussion

By analyzing the change in hardness and microstructure with aging temperature (see Table 1 and Fig. 1), we can divide the aging of Custom 465® into three major stages: peak aging, overaging, and progressive overaging. Upon aging of Custom 465®, the microstructure is modified by two mechanisms: precipitation and growth of a stable η-Ni_3Ti phase, and reversion of martensite to austenite. The first stage is the maximal aging hardening obtained after 4 h at 480–510 °C. Both η-Ni_3Ti precipitation and reverted austenite transformation begin independently of each other. The formation of austenite does not stem from the precipitation of Ni_3Ti. The second stage is overaging, which is observed in specimens aged for 4 h at 538 °C and 560 °C, and is associated with a minor hardness decrease. Both the diameter of precipitates and the volume fraction of reverted austenite slightly increase in the second stage. The third stage is progressive overaging observed in all samples aged for 4 h above 593 °C. This stage is characterized by a substantial hardness decrease due to the significant increase both in the dimensions of precipitates and in the volume fraction of reverted austenite.

The thermodynamic calculations yielded several conclusions, which do not take into account any kinetic effects. First, both phases are competing for the Ni atoms, thus the formation of austenite is slightly hindered by the η-Ni_3Ti precipitation. Second, the formation of η-Ni_3Ti occurs prior to the massive formation of reverted austenite, and the amount of the latter is predicted to increase sharply at temperatures lower than the predicted dissolution temperature of η-Ni_3Ti. This is unlike other precipitation-hardened steels, such as C250 steel, where metastable precipitates are formed at the initial stages of aging, and their dissolution at more advanced stages induces local compositional modifications that induce the formation of austenite [3]. The dissolution of precipitates that is predicted to occur above 600 °C can contribute to the formation of reverted austenite by locally increasing the Ni concentration, as suggested by Schnitzer et al. [12] for 13–8Mo PH steel. Our conclusions are in line with those of Sinha et al. [17] who excluded the mechanism of dissolution of precipitates in the formation of reverted austenite and suggested that Ni diffuses to dislocations, resulting in micro-segregation of Ni and local reversion of martensite. Third, austenite formed at lower temperature is richer in Ni and other alloying elements. Although thermodynamic calculations indicate that the amount of reverted austenite is sharply increasing above ~580 °C, similar amounts of reverted austenite were measured at room temperature after aging at 593 °C and 648 °C. This behavior can be explained by the change in austenite composition as a function of aging temperature, which affects the stability of austenite against martensitic transformation. The calculations imply that although more austenite is formed during heating to 648 °C, more of it transforms to martensite upon cooling. This phenomenon was observed in other PH steels as well, but to the best of our knowledge no explanation based on thermodynamic calculations was given. In 13–8Mo PH martensitic stainless steel the volume fraction of reverted austenite increased to similar values until a maximal value was obtained at an aging temperature of 650 °C [26], in Fe-13Cr-4Ni-Mo alloy at 610 °C [27], and in Fe-13Cr-7Ni-3Si at 620 °C [28]. Also, a similar dependency was reported with regard to the dwell time at the aging temperature [18]. These behaviors were attributed to the diffusion-related austenite reversion transformation: increasing either the aging temperature or dwell time results in improved homogeneity, lower maximal Ni concentration, and higher Fe concentration within each austenite patch, and thus the austenite stability is reduced [28]. We suggest, based on our thermodynamic calculations, that the Ni content in austenite decreases as the aging temperature increases, leading to a reduction in its stability at lower temperatures during cooling to room temperature. Hence, diffusion is not necessary for reducing the austenite stability, but may promote the homogeneity of Ni distribution within the austenite.

The two-phase transformations that occur upon aging at 482–648 °C affect the mechanical properties, namely hardness in the current study, in different ways. The non-linear and non-parabolic dependence of hardness on aging temperature, observed in this study, is worth noting. The main explanation to this phenomenon is the opposite effects of the phase transformations occurring nearly simultaneously during aging, namely precipitation of Ni_3Ti and austenite reversion. The strength and hardness change as a function of precipitate size in a parabolic-like manner [4], reaching a maximum at a certain value, and then decreasing. In contrast, the dependency on the amount of austenite is monotonic: increasing the amount of reverted austenite increases the fracture toughness, but reduces the strength and hardness. Within the temperature range of 482–538 °C, the amount of reverted austenite is nearly constant (<5.1 vol%), and it is dispersed as discrete particles. The precipitate dimensions, on the other hand, increase noticeably within this temperature range. Thus, the observed hardening is attributed to precipitates growth; the precipitate dimensions that yield a maximum strengthening effect (i.e. maximum hardness) are those achieved after 4 h aging at 510 °C. As aging proceeds, the precipitates' dimensions and the austenite volume fraction increase, the latter being reflected by a thin layer along grain boundaries and lamellae boundaries. Both behaviors result in a continuous reduction in hardness [29]. It should also be noted that the hardness (and other mechanical properties) of austenite may also change with aging temperature due to the change in Ni-content in the austenite, the decrease of which leads to softening of the austenite phase.

5. Conclusions

The microstructure and hardness of Custom 465® precipitation hardened stainless steel were characterized following aging at temperatures ranging from 480 °C to 648 °C. Three major stages of aging were observed. The first stage is the hardening at aging temperatures of 480–510 °C, where both η-Ni_3Ti precipitation and austenite reversion begin independently of each other. The second stage is the initial stage of overaging observed above 538 °C, where the reduction in hardness is attributed to a slight increase in both the precipitate dimensions and the austenite volume fraction. The third, progressive overaging stage,

which occurs above 593 °C, is caused by the significant increase in precipitate dimensions and reverted austenite volume fraction. Thermodynamic calculations indicate that the reversion of austenite is not governed by the dissolution of η-Ni_3Ti precipitates, although both phases are in competition for Ni atoms. Although the thermodynamic calculation predicts increase in the fraction of reverted austenite with increase in aging temperature, the fraction of austenite found in quenched samples does not vary when the aging temperature is increased above 593 °C. This is explained by the change in composition of the austenite as a function of aging temperature, which becomes lower in Ni as aging temperature increases. This change in austenite composition may also be manifested in hardness reduction.

Acknowledgements

This work was supported by Grant No. 205-13 from the Pazy Foundation. We thank Dr. Dimitri Mogiliansk and Prof. Amit Kohn for their guidance and helpful comments, and Mr. Shlomo Levi, Mr. Michael Amos and Mr. Yair George for their technical assistance.

References

[1] D.E. Wert, R.P. DiSabella, Strong, corrosion-resistant stainless steel, Adv. Mater. Process. 164 (2006) 34–36.
[2] S. Ifergane, E. Sabatani, B. Carmeli, Z. Barkay, V. Ezersky, O. Beeri, N. Eliaz, Hydrogen diffusivity measurement and microstructural characterization of custom 465 stainless steel, Electrochim. Acta 178 (2015) 494–503.
[3] O. Moshka, M. Pinkas, E. Brosh, V. Ezersky, L. Meshi, Addressing the issue of precipitates in maraging steels - unambiguous answer, Mater. Sci. Eng. A 638 (2015) 232–239.
[4] W. Sha, Z. Guo, Maraging Steels: Modelling of Microstructure, Properties and Applications, first ed. Woodhead Publishing Ltd., New Delhi, India, 2009.
[5] W. Sha, A. Cerezo, G.D.W. Smith, Phase chemistry and precipitation reactions in maraging steels: part IV. Discussion and conclusions, Metall. Trans. A 24A (1993) 1251–1256.
[6] Y. He, K. Yang, W. Sha, Microstructure and mechanical properties of a 2000 MPa grade Co-free maraging steel, Metall. Mater. Trans. A 36 (2005) 2273–2287.
[7] D.M. Vanderwalker, The precipitation sequence of Ni_3Ti in Co-free maraging steel, Metall. Trans. A 18A (1987) 1191–1194.
[8] V.K. Vasudevan, S.J. Kim, C.M. Wayman, Precipitation reactions and strengthening behavior in 18 wt% nickel maraging steels, Metall. Trans. A 21 (1990) 2655–2668.
[9] E.V. Pereloma, A. Shekhter, M.K. Miller, S.P. Ringer, Ageing behaviour of an Fe–20Ni–1.8Mn–1.6Ti–0.59Al (wt.%) maraging alloy: clustering, precipitation and hardening, Acta Mater. 52 (2004) 5589–5602.
[10] J.I. Suk, S.H. Hong, S.W. Nam, Crystallographic orientation relationships among η-Ni_3Ti precipitate, reverted austenite, and martensitic matrix in Fe-10Cr-10Ni-2W maraging alloy, Metall. Trans. A 24 (1993) 2643–2652.
[11] A. Shekhter, H.I. Aaronson, M.K. Miller, S.P. Ringer, E.V. Pereloma, Effect of aging and deformation on the microstructure and properties of Fe-Ni-Ti maraging steel, Metall. Mater. Trans. A 35 (2004) 973–983.
[12] R. Schnitzer, R. Radis, M. Nöehrer, M. Schober, R. Hochfellner, S. Zinner, E. Povoden-Karadeniz, E. Kozeschnik, H. Leitner, Reverted austenite in PH 13–8 Mo maraging steels, Mater. Chem. Phys. 122 (2010) 138–145.
[13] E.U. Lee, R. Goswami, M. Jones, A.K. Vasudevan, Environment-assisted cracking in Custom 465 stainless steel, Metall. Mater. Trans. A 42 (2011) 415–423.
[14] Custom 465® Stainless Steel, Technical Datasheet, Carpenter Company, 2014.
[15] ASTM E975 - 13, Standard Practice for X-ray Determination of Retained Austenite in Steel With Near Random Crystallographic Orientation, ASTM International, (n.d.). West Conshohocken, PA, DOI: 10.1520/E0975-13.
[16] K. Wakasa, C.M. Wayman, Isothermal martensite formation in an Fe-20%Ni-5%Mn alloy, Metallography 14 (1981) 37–48.
[17] P.P. Sinha, D. Sivakumar, N.S. Babu, K.T. Tharian, A. Natarajan, Austenite reversion in 18Ni Co-free maraging steel, Steel Res. 66 (1995) 490–494.
[18] P. Song, W. Liu, C. Zhang, L. Liu, Z. Yang, Reversed austenite growth behavior of a 13%Cr-5%Ni stainless steel during intercritical annealing, ISIJ Int. 56 (1) (2016) 148–153.
[19] Z. Guo, W. Sha, D. Li, Quantification of phase transformation kinetics of 18 wt.% Ni C250 maraging steel, Mater. Sci. Eng. A 373 (2004) 10–20.
[20] G. Saul, J.A. Roberson, A.M. Adair, The effects of thermal treatment on the austenitic grain size and mechanical properties of 18 Pct Ni maraging steels, Metall. Trans. 1 (1970) 383–387.
[21] R. Kapoor, I.S. Batra, On the α' to γ transformation in maraging (grade 350), PH 13–8 Mo and 17–4 PH steels, Mater. Sci. Eng. A 371 (2004) 324–334.
[22] K.W. Andrews, Empirical formulae for the calculation of some transformation temperatures, J. Iron Steel Inst. 203 (1965) 721–727.
[23] J.O. Andersson, T. Helander, L. Höglund, P.F. Shi, B. Sundman, Thermo-Calc and DICTRA, computational tools for materials science, CALPHAD 26 (2002) 273–312.
[24] Thermo-Calc Software TCFE7 Steels/Fe-alloys Database Version 7 (n.d.).
[25] P.E.A. Turchi, L. Kaufman, Zi-Kui Liu, Modeling of Ni–Cr–Mo based alloys: part I—phase stability, CALPHAD 30 (2006) 70–87.
[26] X. Li, J. Zhang, J. Chen, S. Shen, G. Yang, T. Wang, X. Song, Effect of aging treatment on hydrogen embrittlement of PH 13–8 Mo martensite stainless steel, Mater. Sci. Eng. A 651 (2016) 474–485.
[27] Y. Song, X.A. Li, L. Rong, Y. Li, The influence of tempering temperature on the reversed austenite formation and tensile properties in Fe–13%Cr–4%Ni–Mo low carbon martensite stainless steels, Mater. Sci. Eng. A 528 (2011) 4075–4079.
[28] D.S. Leem, Y.D. Lee, J.H. Jun, C.S. Choi, Amount of retained austenite at room temperature after reverse transformation of martensite to austenite in an Fe-13%Cr-7%Ni-3%Si martensitic stainless steel, Scr. Mater. 45 (2001) 767–772.
[29] W. Sha, Steels: From Materials Science to Structural Engineering, Springer-Verlag, London, 2013, http://dx.doi.org/10.1007/978-1-4471-4872-2.